Reliable Metal Foreign Object Detection for Mobile Wireless Charging via Harmonic Fingerprinting

Shenyao Jiang
City University of Hong Kong
China
sjiang86-c@cityu.edu.hk

Yang Liu
Florida State University
USA
yl25r@fsu.edu

Lixiang Han
City University of Hong Kong
China
lxhan2-c@cityu.edu.hk

Xinyu Wang
University of Science and Technology of China
China
xinyuwang0306@ustc.edu.cn

Hao Zhou
University of Science and Technology of China
China
kitewind@ustc.edu.cn

Zhenjiang Li
City University of Hong Kong
China
zhenjiang.li@cityu.edu.hk

Abstract

Wireless charging eliminates cumbersome cables, revolutionizing how to charge mobile devices, yet reliably detecting metal foreign objects (e.g., keys, SIM ejectors, paper clips) poses a persistent challenge. This detection is critical, as such objects can inadvertently enter the charging zone, absorb energy, and trigger overheating, diminished efficiency, device damage, and even burns or fires. Existing approaches mainly monitor energy loss at the mobile device to infer intrusions, but this loss mixes inherent system dissipation with object-induced effects, both highly variable across devices and conditions, which often results in missed detections (as found in a range of commercial chargers). In this paper, we present MetSentry, a novel system design that takes a fundamentally different approach. Our key insight is that, beyond energy absorption, metal foreign objects also alter the electromagnetic field: they disproportionately attenuate the high-frequency harmonics in the in-band communication waveforms during charging, acting as a low-pass filter and yielding a distinctive, physics-grounded fingerprint of their presence. MetSentry captures and analyzes these fingerprints through a lightweight sensing circuit and a tailored software pipeline that extracts robust, discriminative features, which can be seamlessly integrated into wireless chargers, enabling reliable detection. Extensive experiments with various commercial wireless chargers, smartphones, and metal foreign objects demonstrate that MetSentry consistently outperforms both built-in charger detection and state-of-the-art methods.

CCS Concepts

• **Hardware** → **Power and energy**; • **Computer systems organization** → *Embedded and cyber-physical systems.*

Keywords

Wireless charging, foreign object detection, harmonic fingerprinting, contrastive learning, mobile sensing

MobiSys '26, June 21–25, 2026, Cambridge, United Kingdom

ACM ISBN 979-8-4007-2027-7/2026/06
https://doi.org/10.1145/3745756.3809222

ACM Reference Format:
Shenyao Jiang, Yang Liu, Lixiang Han, Xinyu Wang, Hao Zhou, and Zhenjiang Li. 2026. Reliable Metal Foreign Object Detection for Mobile Wireless Charging via Harmonic Fingerprinting. In *The 24th Annual International Conference on Mobile Systems, Applications and Services (MobiSys '26), June 21–25, 2026, Cambridge, United Kingdom.* ACM, New York, NY, USA, 15 pages. https://doi.org/10.1145/3745756.3809222

1 Introduction

Wireless charging, which delivers energy through an electromagnetic field, has revolutionized how mobile devices are charged by enabling seamless, contactless energy transfer between a charger and a device [6, 9, 10]. With over 80% of flagship phones now supporting this technology [39] and projections exceeding $165 billion by 2034 [50], wireless charging is swiftly becoming ubiquitous in consumer electronics, offices, homes, cars, malls, etc.

Safety is the cornerstone of wireless charging, and modern standards treat *metal foreign object detection (FOD)* as a **mandatory safety mechanism** [8, 32]. Everyday items like keys, coins, SIM ejectors, and NFC or transit cards can inadvertently enter the charging zone, *e.g.*, when placed inside phone cases, attracted by alignment magnets, or simply overlooked on charging surfaces as users increasingly integrate chargers into cars, offices, kitchens, and public spaces. Such objects absorb electromagnetic energy and can heat rapidly, posing risks of burns, device damage, or even fires.

To avoid these dangers, global regulations including IEC 62368-1 [8], GB/T 38775 [34], and the Qi2 [10] standards require chargers to detect foreign metals **before** the object temperature exceeds 70 °C (beyond which risks may occur), and mandate ignition tests across more than a dozen metal object configurations [8, 10]. Despite these clear requirements, our measurements of 10 popular chargers across Asia, Europe, and North America show that most fail to meet this threshold, allowing common metal objects to reach 90 °C to 150 °C without triggering detection (§2). As wireless charging continues to proliferate into homes, vehicles, industrial sites, and other metal rich or safety sensitive environments [24], closing this detection gap is not only a technical challenge, but also an urgent and under-recognized safety demand.

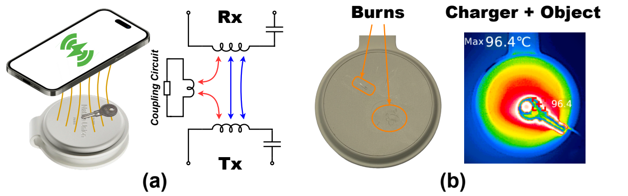

Figure 1: (a) A metal foreign object present in the charging zone will introduce an additional coupling circuit to absorb energy. (b) A showcase of an undetected metal foreign object using a commercial wireless charger, leading to overheating up to 96.4°C captured by a thermal imaging camera and deformation of the charger.

Understanding why these failures occur requires examining how existing detection mechanisms work. When a foreign object[1] enters the charging zone, it creates an additional (parasitic) coupling circuit between the charger (Tx) and the mobile device (Rx) to absorb energy, consisting of *resistive* and *inductive* elements [30], as illustrated in Figure 1(a). Prevailing approaches detect these intrusions primarily by monitoring energy loss (or related parameters, detailed in §7) at the Tx [10, 30]. The core challenge lies in the complex combination of the system's inherent energy dissipation and object-induced effects. Inherent dissipation varies with receiver model, coil alignment and power level, while object-induced effects hing on the object's material, geometry and position. Because their combined effect is highly variable, many commercial wireless chargers *employ overly conservative detection thresholds that favor uninterrupted charging over safety.* Consequently, missed detections are alarmingly common, as shown in Figure 1(b).

To overcome these limitations, we take a different perspective in this paper by exploiting distinctive fingerprints of metal foreign objects in the charging zone for reliable detection. In addition to energy delivery, the electromagnetic field also serves as a communication channel, allowing mobile devices to periodically transmit status updates to the charger [52]. These packets are encoded by modulating the field's amplitude into a square-wave sequence through load adjustments at the device (detailed in §2). When a metal object appears, its resistive element uniformly attenuates the electromagnetic field across frequencies, while the inductive element selectively suppresses high-frequency harmonics.

Drawing on Fourier analysis, square-wave signals are inherently rich in high-frequency harmonics at their transitional edges. We observe that a foreign object's inductive element acts as a **low-pass filter**, smoothing these edges into **rounded, sine-like** waveforms dominated by *low-frequency components*. This phenomenon yields a physics-grounded, distinctive harmonic signature that enables precise detection – far superior to the empirical, threshold-based approximations of prior methods. By inspecting these unique fingerprints, our approach achieves markedly higher accuracy and reliability. Leveraging this insight, we tackle two problems:

1) Reliable harmonic sensing. We propose integrating a low-cost planar sensing coil array into the wireless charger, optimized to capture electromagnetic field waveforms rich in harmonic details. As a proof-of-concept, we fabricate it using a copper trace printed on a PCB. The high-impedance coil design ensures that the array itself does not become a foreign object. Commercial chargers can easily adopt this design by allocating modest PCB space during manufacturing.

[1]We sometimes refer to metal foreign objects simply as foreign objects.

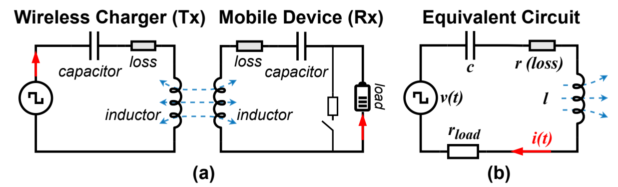

Figure 2: (a) Individual circuits of Tx and Rx. (b) Equivalent wireless charging circuit (without foreign objects).

2) Robustness across real-world conditions. Even with cost-effective hardware, detection must cope with real-world variability, including different object positions, charging power levels, and unseen metal items. Since it is impractical to anticipate all such variations, we adopt a simple contrastive learning strategy that focuses on distinguishing foreign-object fingerprints from normal charging patterns. This keeps the approach lightweight while maintaining reliable detection without exhaustive data collection.

We integrate this hardware-software co-design into a comprehensive system, MetSentry, and prototype it for evaluation. Our hardware employs three compact sensing coils for spatial diversity, fabricated as concentric 0.8 mm copper traces with radii spanning 10–19 mm. Deployed across 14 commercial wireless chargers, we evaluate MetSentry with various popular smartphones and 11 common metal foreign objects (detailed in §5). Results reveal that 11 out of these 14 chargers rarely detect foreign objects before the 70 °C safety threshold by existing methods, while MetSentry successfully detected all cases. It outperforms built-in commercial detection mechanisms by 75.9–86.6% and the state-of-the-art academic method by 35.1–77.0%. Crucially, MetSentry detects foreign objects at an average temperature of just 32.8 °C, far below safety thresholds. Micro-benchmarks confirm its robustness across varied scenarios. The paper's contributions are summarized below.

- We discover a significant safety hazard of missed detection for metal foreign objects on commercial wireless chargers, identify the reason, and find and leverage a novel physics-grounded fingerprint for reliable detection.
- We present MetSentry, a full-stack solution comprising low-cost sensing coils optimized for electromagnetic signal acquisition and a software pipeline tailored for efficient preprocessing and metal foreign object detection.
- We conduct experiments across multiple commercial wireless chargers and smartphones, demonstrating that MetSentry significantly outperforms commercial and state-of-the-art methods in detecting metal foreign objects across our evaluated test set.

2 Background and Observation

2.1 Wireless Charging and Foreign Objects

(1) Overview of Wireless Charging. As illustrated in Figure 2(a), the wireless charging modules in the charger (Tx) and the mobile device (Rx) each have dedicated charging circuits. The Tx generates an alternating current that flows through its coil (inductor), producing an alternating electromagnetic field. Through electromagnetic induction, this field induces a corresponding current in

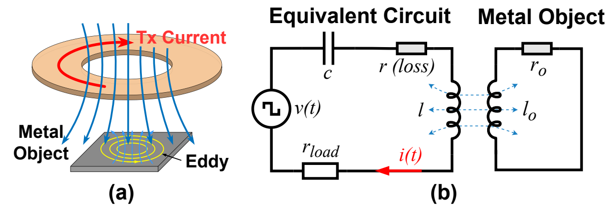

Figure 3: (a) Eddy currents induced inside the foreign object. (b) Equivalent circuit with the metal object.

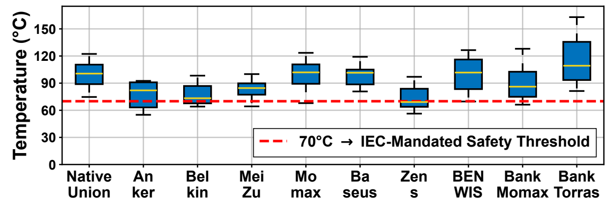

Figure 4: Temperature distribution when detecting foreign objects on various commercial wireless chargers. Most chargers fail to identify foreign objects before their temperature exceeds the IEC-mandated safety threshold of 70 °C.

the Rx inductor, which then flows in the Rx circuit to charge device's battery (load).

This process can be represented as the simplified **equivalent circuit** in Figure 2(b), comprising three essential parts:

- **Excitation current** $i(t)$: The alternating current driven by the Tx's alternating voltage $v(t)$, which generates the electromagnetic field.
- **Impedance** (r, l, c): A compact representation of Tx and Rx circuits' combined behavior. Here, r models resistive losses from Tx and Rx, while l and c reflect the equivalent inductive and capacitive properties of the Tx and Rx.
- **Load** r_{load}: The effective resistance of Rx's load, primarily the battery, and $i(t)$ flows through r_{load} to charge the battery.

(2) Metal Foreign Objects. Metal objects commonly found near mobile devices include SIM ejectors, paper clips, coins, and contactless chip cards. These items are typically small and thin. With the widespread use of wireless chargers in more and more aspects of our daily life (*e.g.*, homes, cars, and public sites), such objects can easily get into charging zones (*e.g.*, placed inside phone cases, attracted by alignment magnets in the charger, or placed on dark, cluttered surfaces) and remain there for extended periods, but users may habitually charge their phones without noticing them [23].

Consequences. The electromagnetic field induces eddy currents within these objects [35] (Figure 3(a)), leading to overheating, often reaching 70–100 °C or higher. This not only squanders energy, diminishes charging efficiency, and extends charging durations but also risks damaging sensitive electronic components and causes severe dangers like burns, fires, or explosions [30, 52, 62]. Such risks will intensify in (increasingly prevalent) interconnected setups (*e.g.*, in-car phone charging and shared charging trays) and metal-rich or safety-sensitive environments (*e.g.*, warehouses and industrial sites), where a single risk could cascade into catastrophe.

Safeguard requirements. The International Electrotechnical Commission (IEC) establishes rigorous safety standards for electronic devices [8]. In particular, IEC 62368-1 defines a thermal limit of 70 °C for accessible parts and requires that equipment prevent metal foreign objects from exceeding this threshold. Consistent with this, global wireless power standards like GB/T 38775 [34], and the Qi protocol family [10] treat foreign object detection as a fundamental safety function: they require chargers to detect foreign metals *before* the object temperature exceeds 70 °C, and mandate ignition tests across more than a dozen representative metal object configurations [10, 34]. Since the electromagnetic field attenuates rapidly outside the charging zone, the influence of nearby metal objects is small. Therefore, the IEC standard and Qi2 compliance only focus on detecting metal foreign objects within the charging zone [8, 10].

(3) Difficult of Detection. Despite these clear safeguard requirements, reliably detecting metal foreign objects in practice remains challenging. To understand why, we first examine a foreign object's impact on the charging system. In Figure 3(a), eddy currents in the object generate a secondary electromagnetic field that distorts the original charging field. Circuit-wise, this equates to introducing an additional coupling component into the equivalent charging circuit, with a resistor r_o and an inductor l_o (Figure 3(b)). The overall circuit equation retains the form from Figure 2(b):

$$v(t) = (r' + j\omega l' + \frac{1}{j\omega c} + r_{load}) \times i(t), \tag{1}$$

but with r' and l' modified by the metal foreign object:

$$r' = r + \beta \times r_o, \text{ and } l' = (1 + \alpha) \times l + \beta \times l_o, \tag{2}$$

where r and l are the baseline resistance and inductance without the foreign object, and α and β capture the coupling dynamics between the foreign object and the Tx-Rx circuit.

- Coefficient α reflects the strength of coupling between the object and the Tx-Rx circuit, influenced by the object's material properties such as conductivity and geometry.
- Coefficient β accounts for the induced eddy currents and field superimposition, varying with the object's position and the number of objects in the charging zone.

Commercial methods. Existing commercial wireless chargers typically rely on measures of energy loss for detection [9, 32]. While foreign objects indeed absorb energy, accurately quantifying this loss demands estimating the unknown coupling parameters such as coefficients α and β. Moreover, variations in device models, coil coupling, and power levels further influence the current $i(t)$, rendering precise estimates infeasible in practical settings. Hence, commercial systems resort to conservative detection thresholds for energy loss, which minimize disruptive false positives but often delay detection, increasing the likelihood that metal objects remain unnoticed until the temperature rises beyond safety limits.

To understand the shortcomings of existing methods, we perform a preliminary experiment on nine commercial wireless chargers. For each, we position a metal object at ten varied locations within the charging zone and use K-type thermocouple sensors for real-time surface temperature monitoring and recording the temperature at detection. Figure 4 shows that these chargers rarely detect foreign objects before their temperature exceeds the IEC-mandated safety threshold of 70 °C. Detection frequently occurs

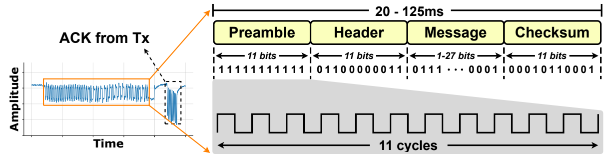

Figure 5: Example of a wireless charging data packet: the electromagnetic field amplitude is modulated into a square wave for transmission.

only at dangerously high temperatures, with an average of 93.3 °C and worst-case delays pushing beyond 150 °C. These findings underscore the inadequacy of energy loss-based approaches in safeguarding wireless charging reliability and user safety.

Other methods. Other methods, like monitoring other relevant circuit parameters or using on-device (temperature) sensors, also present similar problems (see §6).

2.2 Design Observation

(1) Communication in Wireless Charging. During wireless charging, the mobile device regularly feeds back status updates to the charger, reusing the same electromagnetic field through amplitude modulation.

Specifically, the charging module on the mobile device (Rx) includes an on-off switch in parallel with the main load, as shown in Figure 2(a). By toggling this switch, the device creates a temporary current path that alters the effective load impedance, modulating the current drawn from the charger and reshaping the electromagnetic field's amplitude into a square-wave pattern. Data is then encoded in this square wave via differential bi-phase encoding [52] (a variant of Manchester coding). Figure 5 exemplifies one such packet, with the following key properties:

- **Packet format**: A preamble (at least 11 cycles) followed by a header, payload (message), and checksum. Packet duration is typically 20–50 ms depending on message length.
- **Packet interval**: The interval between two data packets normally ranges from tens to hundreds of milliseconds.
- **Fundamental frequency**: 2 kHz, each bit lasting 500 μs.

(2) Opportunity: Harmonic Fingerprints. A square-wave signal is inherently rich in harmonic components — its sharp edges introduce higher-frequency components that are integer multiples of the fundamental frequency, essential for maintaining the waveform's square shape. On the other hand, during wireless charging, the charger dynamically adjusts its capacitance to make the equivalent circuit's capacitance c and inductance l match (as in Figure 2(b)), targeting for LC resonance to cancel reactive impedance. This tuning directs most of the current $i(t)$ toward the load r_{load}, maximizing efficiency while minimizing distortions to the electromagnetic field. Consequently, in the absence of metal foreign objects, sensed electromagnetic field envelopes during packet transmission exhibit pronounced square-wave characteristics.

In contrast, a metal object's intrusion introduces parasitic inductance, disrupting the LC balance and leaving residual inductive reactance. Inductors naturally attenuate high frequencies, so this mismatch acts as an effective low-pass filter. As a result, the sensed electromagnetic field envelope during packet transmission tends to lose its sharp edges, with higher harmonics suppressed,

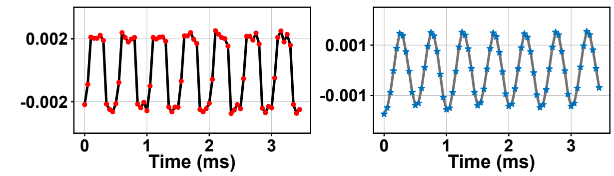

Figure 6: (a) Without foreign object, the signal amplitude envelope is square-waved, slightly distorted by imperfect LC tuning and device interference; (b) The presence of foreign object yields a sine-like envelope.

degrading into a smoother, sinusoidal waveform dominated by the fundamental frequency.

We empirically validate this effect. As shown in Figure 6(a), without a foreign object, the envelope of a wireless charging data packet retains a distinct square-wave form, with minor deviations from imperfect LC tuning and weak coupling of electronic components inside the phone. Conversely, Figure 6(b) demonstrates that a foreign object's presence suppresses harmonics, producing a sinusoidal-like envelope (because higher harmonics are not completely suppressed, there are slight differences from the ideal sine wave).

This observation reveals a key opportunity: rather than relying on unknown Tx-Rx parameters or variable energy-loss metrics, we can robustly detect foreign objects by monitoring the characteristic suppression of higher-order harmonics in communication signals. The unique patterns of this suppression provide a device-agnostic, highly discriminative fingerprint, enabling consistent and accurate detection across varied chargers, devices, and object types.

(3) Design Overview. Building on this observation, we develop MetSentry through two synergistic designs, providing a lightweight and cost-effective choice for integration into wireless chargers: 1) **Sensing hardware platform**: Customized sensing coils and optimized circuits to capture high-quality electromagnetic field signals, preserving harmonic details without interfering with normal charging operations (§3); 2) **Detection software pipeline**: A tailored pipeline that preprocesses sensed signals and leverages harmonic fingerprints for robust metal foreign object detection (§4). Wireless charger manufacturers, the primary target adopters of MetSentry, can leverage our design to improve their chargers.

3 Sensing Hardware Platform

To harness harmonic fingerprints for foreign object detection, MetSentry requires a hardware platform to capture electromagnetic communication signals with sufficient fidelity.

3.1 Hardware Design

Figure 7 shows an overview of our hardware design with two main components: 1) sensing coils and 2) a signal extractor. The sensing coils capture the time-varying electromagnetic field, while the extractor circuit converts raw coil signals into clean harmonic fingerprints suitable for detection.

(1) Sensing Coils. Conventional magnetic sensors provide calibrated absolute flux measurements but require complex circuitry, large form factors, and high power, and are typically limited to low-frequency operation (75 Hz for HMC5883L [25]), making them unsuitable for capturing the high-frequency harmonics needed for

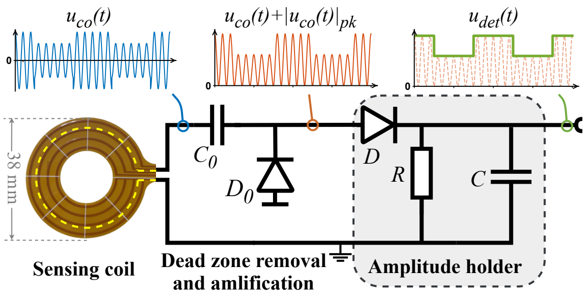

Figure 7: Hardware design with sensing coils (left) and the corresponding extractor circuits (right) to obtain envelop waveforms containing harmonic fingerprints.

foreign object detection [25, 60]. Instead, we only need relative variations in the electromagnetic field, specifically the harmonic components of the 2 kHz communication signal, and therefore adopt a planar sensing coil whose Faraday-law-induced voltage directly exposes these modulation patterns and harmonic distortions. Since wireless charging requires continuous communications between the charger and the mobile device, the sensing fingerprint can be consistently obtained, enabling uninterrupted detection.

1.1) Design. We develop a planar circular sensing coil that directly picks up the magnetic field with minimal latency and wide bandwidth. As a proof of concept, the coil is fabricated as a copper trace on a thin flexible printed circuit board (PCB). For practical deployment, commercial chargers can reserve a small portion of PCB space to integrate the sensing coil, without requiring additional PCB layers. The total additional hardware cost, including the extraction circuit, is about \$5, which becomes negligible when mass-produced and integrated at the PCB level. This offers a lightweight and cost-effective choice for integration into wireless chargers.

Will the sensing coil itself be a foreign object? No. The high input impedance of the subsequent detection circuit limits the induced current in the coil to μA levels, ensuring that the sensing coil itself does not become a heat-generating object. As shown in Figure 8, over 90 seconds of charging, the temperature curve of our sensing coil ("with coil") almost overlaps the temperature change at the same location without the coil ("without coil"), whereas a metal foreign object causes the temperature to over 90 °C ("with object"). This indicates that our sensing coil does not behave as a heat-generating object and ensures safety compliance.

1.2) Sensing Principle. When exposed to the electromagnetic field of the charger, the sensing coil experiences a changing magnetic flux Φ, which induces a voltage across the coil according to Faraday's law. MetSentry uses this induced voltage $u_{co}(t)$, which can be expressed as:

$$u_{co}(t) = \gamma \frac{\partial \Phi}{\partial t} = \gamma \frac{\partial (A \times B(t))}{\partial t}, \tag{3}$$

where A is the area covered by the sensing coil, $B(t)$ is the magnetic field strength, and γ is a proportionality constant.

Because the magnetic field $B(t)$ is directly related to the excitation current $i(t)$ in the equivalent charging circuit (detailed by Eqn. (11) in §3.2), the induced voltage $u_{co}(t)$ can reflect the harmonic content of $i(t)$. In other words, the sensing coil transforms variations in the charging field into a measurable voltage signal, from which we can extract the harmonic fingerprints needed for foreign object detection. In principle, a wireless charger can reuse its charging coil for detection (similar to a dedicated sensing coil), but the performance is limited due to insufficient spatial diversity.

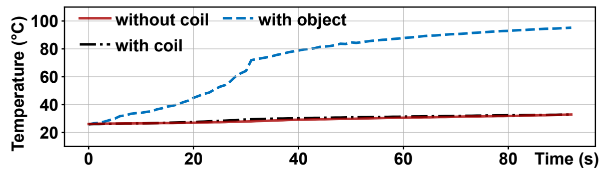

Figure 8: Temperature changes over time under three conditions to demonstrate that our sensing coil itself will not become a heat-generating foreign object.

1.3) Spatial Diversity. Beyond single-coil sensing, MetSentry also leverages spatial diversity to improve robustness. The sensing coil in our design is circular, which not only simplifies circuit integration but also allows multiple coils to be placed concentrically as an array with minimal overhead (Figure 7(left)). This arrangement requires no extra deployment space yet enables simultaneous measurements at slightly different positions in the electromagnetic field. Each coil of different radii operates independently and outputs its own $u_{co}(t)$ signal, covering different areas within the charging zone and providing multiple perspectives of the same charging process. These parallel channels enhance the likelihood of capturing spatial distortions caused by foreign objects and improve detection performance than using one coil. The number of coils can be adjusted, and we empirically use 3 by default (§6.3).

(2) Signal Extractor. The sensing coil output $u_{co}(t)$ contains both the 2 kHz communication signal and 360 kHz power carrier, producing a composite waveform from which harmonics need to be extracted. If we directly sample the signal to extract the desired frequency components, processing such high-rate streams can quickly overwhelms resource-constrained processors, especially when multiple coils are used, leading to buffer overflows and data loss.

2.1) Extracting envelope. Since the harmonic fingerprints we require appear in the low-frequency 2 kHz envelope of the communication signal, we design a lightweight circuit that directly extracts this envelope, as depicted in Figure 7. A classic envelope detector (diode plus low-pass filter) uses a diode (D), resistor (R), and capacitor (C), but it cannot be applied directly here: the diode only conducts when the input exceeds its forward voltage (about 0.27 V), which would cause weak yet informative harmonic components to be lost. To overcome this limitation, we extend the circuit design so that even low-amplitude signals can be preserved, ensuring reliable capture of harmonic fingerprints for detection.

2.2) Enhanced extractor. MetSentry extends the classic envelope detector with two key enhancements:

- *Dead zone removal*: We add an auxiliary diode (D_0) with 0.5 V forward bias in parallel with the sensing coil. This configuration establishes a DC bias current path that maintains the main diode D in a pre-conduction state, enabling the classic envelope detector to function as an *amplitude holder*, as shown in Figure 7. Hence, D does not fully switch off during weak inputs, and the signal ($u_{co}(t)$), although small, can still pass through to the amplitude holder for envelope extraction. This eliminates the dead zone caused by the diode's forward voltage and ensures that weak harmonic components are preserved rather than lost.

- *Capacitor-assisted amplification*: For very small input amplitudes, the extracted envelope can still be too weak, reducing detection reliability. To mitigate this, we place an additional capacitor (C_0) in series with the sensing coil as shown in Figure 7. This capacitor blocks DC (D_0) while creating a charge-pump effect that enhances the AC signal amplitude presented to diode D, i.e., boosting its input voltage from $u_{co}(t)$ to $u_{co}(t) + |u_{co}(t)|_{pk}$, where $|u_{co}(t)|_{pk}$ is the peak amplitude. Since the negative portion of $u_{co}(t)$ cannot pass through diode D, its effect is equivalent to adding $|u_{co}(t)|_{pk}$ to the amplitude, as shown in Figure 7. This improves envelope detection for weak signals.

To maximize envelope detection performance, R and C in the amplitude holder are critical and should satisfy [40]:

$$(5 \sim 10) \times \frac{1}{f_o} \leq R \times C \leq \frac{1 - d_m}{2\pi f_a \times d_m}, \tag{4}$$

where d_m is the modulation depth (typically 0.05). Based on f_o = 360 kHz and f_a = 2 kHz in wireless charging, we set $R = 5.6\,\mathrm{k\Omega}$ and $C = 10\,\mathrm{nF}$ in MetSentry.

3.2 Signal Analysis

The output $u_{det}(t)$ of the circuit in Figure 7 tracks the varying of the upper envelop of a variant of the sensing coil's output $u_{co}(t) + |u_{co}(t)|_{pk}$. This output approximates the shape of the square-wave amplitude while preserving the effects of dead-zone removal and capacitor amplification. To confirm that $u_{det}(t)$ still retains the harmonic fingerprints needed for foreign object detection, we provide a theoretical analysis and experimental verification.

1) Circuit Output $u_{det}(t)$. In the amplitude holder of Figure 7, the product of resistance (R) and capacitance (C), known as the RC time constant (τ) [41], represents the time duration, wherein the capacitor charges or discharges through the resistor. Therefore, $u_{det}(t)$ can be expressed as:

$$u_{det}(t) \quad = \quad \max_{\tau \in [t-\tau, t]} (u_{co}(\tau) + |u_{co}(\tau)|_{pk}) \times e^{-\frac{t-\tau}{\tau}}, \tag{5}$$

which can be rephrased as follows after we substitute $u_{co}(t)$ (derived below in Eqn. (11)) into the above equation:

$$u_{det}(t) \quad = \quad -\frac{\gamma \mu_0 A K f_o \sin(\frac{\pi T_d}{2})}{\pi(z + r_{load} + \mathrm{H}(\omega))} \times \Big[1 + u_{sq}(t)\Big], \tag{6}$$

where $u_{sq}(t)$ represents a square wave, and T_d is the duty cycle of power source. The complex impedance $H(\omega)$ and other factors in Eqn. (6) will be elaborated below in this subsection. Through Fourier expansion, we can obtain:

$$u_{det}(t) \quad \propto \quad \sum_{n=1}^{\infty} \frac{\sin(n\omega t)}{\hat{\mathrm{H}}(n\omega)}\Bigg|_{\omega = 2\pi f_a}, \tag{7}$$

where $\hat{\mathrm{H}}(n\omega) = z + r_{load} + \mathrm{H}(\omega)$, and the central frequency of square wave is f_a (*i.e.*, 2 kHz).

Eqn. (7) indicates that $u_{det}(t)$ combines multiple sine waves at frequencies "$n \times f_a$", scaled by the inverse of the circuit's frequency response $\hat{\mathrm{H}}(n\omega)$. When a foreign object introduces an inductor, it acts as a low-pass filter, that is, the impedance of this inductor rises with frequency, strongly weakening harmonics ($n \geq 2$) by making $\hat{\mathrm{H}}(n\omega)$ larger. This suppresses high-frequency harmonics, leaving a cleaner signal dominated by the foundation frequency f_a that resembles a wave closer to a sine wave in the time domain.

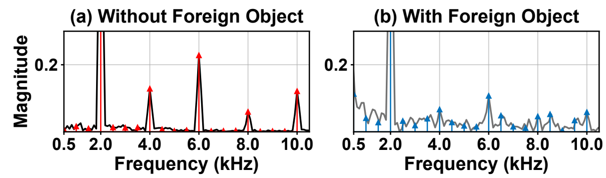

Figure 9: Spectrum of the circuit output $u_{det}(t)$ collected (a) without and (b) with foreign object. For ease of presentation, we normalize the magnitudes to the value of the fundamental frequency of 2 kHz.

Empirical validation. To reveal this, we collect $u_{det}(t)$ with and without foreign object. We compare their spectrum and indeed observe in Figure 9(b) that when there is foreign object, the spectrum shows obvious attenuation at high-order harmonics, *e.g.*, > 2 kHz, compared to Figure 9(a).

2) Sensing Coil Output $u_{co}(t)$. We derive the sensing-coil output $u_{co}(t)$ used in Eqns. (5) and (6). The Tx source $v_{sr}(t)$ is amplitude-modulated by the Rx switching $u_{sq}(t)$ in §3.1:

$$v(t) \quad = \quad v_{sr}(t)\big(u_{sq}(t) + 1\big), \tag{8}$$

where $u_{sq}(t)$ is a square wave $\frac{d_m}{\pi} \sum_{n=1,3,5,\ldots}^{\infty} \frac{\sin(2\pi n f_a t)}{n}$ with depth d_m and f_a = 2 kHz. The equivalent impedance is:

$$\begin{aligned} z' \quad &= \quad (r + j\omega l + \tfrac{1}{j\omega c}) + r_{load} + \big(\beta r_o + j\omega(\alpha l_o + \beta l_o)\big) \\ &= \quad z + r_{load} + H(\omega), \end{aligned} \tag{9}$$

where $H(\omega)$ captures the foreign-object perturbation. Thus the excitation current is:

$$i(t) = v_{sr}(t)\,\frac{u_{sq}(t) + 1}{z + r_{load} + H(\omega)}. \tag{10}$$

By the Biot–Savart law [17] and combining with Eqn. (3), the current $i(t)$ induces:

$$B(t) = \frac{\mu_0}{4\pi} \oint \frac{i(t)\,\hat{\mathbf{r}} \cdot d\mathbf{l}}{r^2}, \text{ and } u_{co}(t) = -\gamma \frac{\mu_0 A}{4\pi} K \frac{\partial i(t)}{\partial t}, \tag{11}$$

where μ_0 is the vacuum permeability, A is the sensing-coil area, and K captures the coil geometry and placement. Substituting above $u_{co}(t)$ into Eqns. (5) and (6) yields $u_{det}(t)$.

4 Software Detection Pipeline

While the output signal $u_{det}(t)$ from our sensing circuit embeds distinctive fingerprints indicative of metal foreign objects, real-world factors like power and device position/load variations can affect the extent of square-wave deviations, consequently impacting detection reliability. To mitigate these influences, we introduce a software detection pipeline.

4.1 Data Preprocessing

Data packets are interspersed within $u_{det}(t)$, with only their amplitude segments being modulated into square waves (§2.2). Thus, we first identify and extract these data packet segments from $u_{det}(t)$ before performing subsequent processing.

(1) Signal Segmentation. Figure 10(a) depicts the amplitude of $u_{det}(t)$ during phone charging, revealing distinct temporal bursts

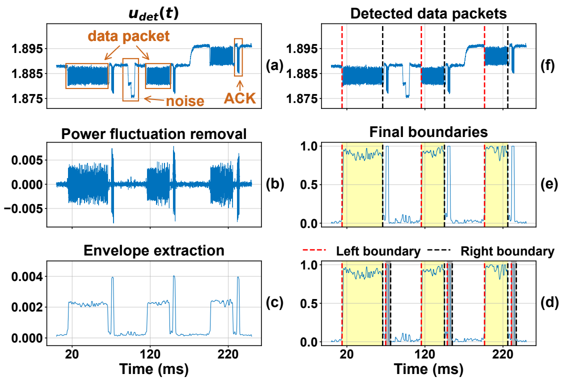

Figure 10: Illustration of the packet segmentation.

where each corresponds to a data packet. After receiving status updates from the phone, the wireless charger may adaptively adjust charging power levels, for instance, incrementally ramping up as seen in Figure 10(a). To achieve precise data packet boundary detection, we design the following preprocessing operations:

- **Power fluctuation removal**: A bandpass filter (*e.g.*, 0.9–9 kHz) eliminates low-frequency artifacts from charging power variations, as shown in Figure 10(b).
- **Envelop extraction**: Sliding window averaging followed by median filtering extracts the signal envelop, effectively highlighting packet structures while suppressing noise, as shown in Figure 10(c) for the output.
- **Boundary detection**: Percentile-based normalization (*e.g.*, 5th–95th percentiles) accommodates amplitude variability, with thresholds (0.5 in MetSentry) pinpointing packet boundaries, as illustrated in Figure 10(d).
- **ACK packet removal**: Enforcing packet duration constraints (400–1200 samples) and minimum packet intervals (300 samples) to filter out ACKs, whose short boundaries fall below the valid duration range (Figure 10(e)).

The detected boundaries are then applied to the original signal (Figure 10(a)) to extract individual packets, as depicted in Figure 10(f). For foreign object detection, we focus on each packet's preamble (the first 11 cycles), which encodes all "1" bits via alternating on/off square waves (§2.2), amplifying the visibility of harmonic fingerprints for detection.

(2) Filtering and Power-Line Noise Suppression. To capture harmonic fingerprints, MetSentry samples the communication signal at 20 kHz, which is sufficient to preserve harmonics up to the 5th order of the 2 kHz square-wave modulation. We then apply a low-pass filter with a 10 kHz cutoff to retain these relevant harmonic components while discarding higher-frequency noise. To further suppress interference, we add a band-stop filter (30–300 Hz) that removes ambient power-line noise at 50 Hz and its several higher-order harmonics [12].

(3) Sensing Coil Array. This preprocessing is applied uniformly to each sensing coil, generating three parallel streams of segmented and filtered $u_{det}(t)$ signals for the subsequent detection module.

4.2 Detection Module

Each preprocessed preamble segment x serves as input to our foreign object detector, which we detail in this subsection. While the distinctive nature of harmonic fingerprints enables strong performance with standard supervised learning (§6.2), we elevate accuracy further by tackling domain diversity through a specialized contrastive learning framework [59].

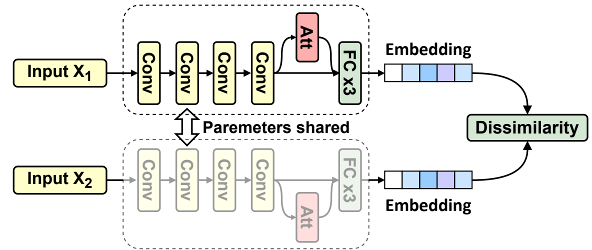

Figure 11: Our dual-branch Siamese detection model.

(1) Domain Diversity. While foreign objects consistently induce a clear trend of signal distortion, the precise extent of square-wave distortion depends on object-related factors, such as material properties, position, and quantity, and device-related variables, like battery level and load dynamics. Ideally, comprehensive coverage of **object-present** samples (*i.e.*, scenarios with foreign objects) would address this diversity, but collecting such an exhaustive dataset is impractical due to the infinite combinations of factors.

To mitigate this, we leverage an inherent asymmetry: **object-free** samples (*i.e.*, scenarios without foreign objects) can be systematically collected offline. This inspires our use of *contrastive learning* to train a detector that maximizes *inter-class distance* between object-present and object-free samples while minimizing *intra-class variance* within each group, yielding a model that generalizes robustly without exhaustive object-present data.

(2) Design. We assemble the object-free sample set $\mathcal{D}^- = \{x_i^-\}_{i=1}^{N^-}$ by randomly sampling N^- instances during offline wireless charging sessions without foreign objects. The object-present set $\mathcal{D}^+ = \{x_j^+\}_{j=1}^{N^+}$ comprises a limited collection of foreign object scenarios. Each sample represents the preamble of one segmented packet.[2] The complete training dataset is denoted as:

$$\mathcal{D} = \{\langle p_i, 0\rangle \mid p_i \in \mathcal{P}_{intra}\} \cup \{\langle p_j, 1\rangle \mid p_j \in \mathcal{P}_{inter}\}, \quad (12)$$

where $\mathcal{P}_{intra} = \{(x_a, x_b) \mid x_a, x_b \in \mathcal{D}^-, a \neq b\}$ represents similar pairs (both object-free), and $\mathcal{P}_{inter} = \mathcal{D}^+ \times \mathcal{D}^-$ denotes dissimilar pairs (differing in foreign object presence). For $\mathcal{P}_{intra}$, we adopt an advanced pair selection strategy [59] prioritizing object-free samples across varied device states (*e.g.*, varied battery levels and loads). This trains the detector to learn inherent commonalities among object-free scenarios under diverse conditions, rather than relying on inconsistent object-present sample similarities.

2.1) Detection model. We design a lightweight Siamese network with twin branches sharing parameters θ to process input pairs $p = (x_1, x_2)$, where x_1 and x_2 are preambles from $\mathcal{D}$. As illustrated in Figure 11, each branch $f_\theta(\cdot)$ comprises four convolutional layers succeeded by fully connected layers. For a given input pair $p = (x_1, x_2)$, the network computes dissimilarity $\hat{y} \in [0, 1]$ by:

$$\hat{y} = \tanh\left(\|f_\theta(x_1) - f_\theta(x_2)\|_2\right), \quad (13)$$

where $\hat{y} \to 0$ indicates similar states (*i.e.*, no foreign object present). We train the network using a modified contrastive loss plus a false

[2] Each sample contains three parallel instances from the three sensing coils, processed identically. We omit coil indices for clarity.

positive penalty:

$$\mathcal{L} = \frac{1}{|\mathcal{D}|} \sum_{\langle p,y \rangle \in \mathcal{D}} \Big[(1-y)\hat{y}^2 + y \max(0, m-\hat{y})^2 + \lambda(1-y)\max(0, \hat{y}-\tau)^2 \Big], \tag{14}$$

where margin m separates dissimilar pairs, tolerance threshold τ controls similar pair boundaries, and λ weights the false positive penalty term. They are empirically set to 0.8, 0.35, and 0.5 in MetSentry, respectively. In §5, we collect a training dataset covering a variety of charging conditions to improve the performance and generaliability of the detection model, which will be further improved by leveraging network architecture search for more suitable architectures and explicit user confirmation for run-time model parameter adaptation in the future.

2.2) Detection. For inference, the Siamese network compares each test signal against a small reference set $\mathcal{D}_r$ consisting of object-free samples from $\mathcal{D}^-$. In MetSentry, we apply k-means clustering with 1% outlier removal to select $n_r = 3$ representative samples as reference templates. Upon receiving a new input x, it is paired with each of n_r templates, and the average dissimilarity score determines decision output: a foreign object is reported if the score exceeds 0.5. To mitigate transient false positive detections, MetSentry aggregates results from three consecutive detections to form a detection cycle and confirms a metal foreign object only when all yield positive outcomes. If a missed detection occurs in the cycle, the next communication packet will automatically trigger a new cycle of detection. In the future, we will explore adjusting the number of consecutive positive detections and the interval between two detection cycles to further improve the detection performance.

5 Implementation

(1) Testbed. We build MetSentry's sensing hardware using readily available commercial off-the-shelf components, ensuring low cost and ease of integration. Each sensing coil is fabricated as a 0.8 mm wide copper trace on a 0.12 mm thick flexible printed circuit board (FPC). As shown in Figure 12, the FPC incorporates multiple concentric coils with radii spanning 10–19 mm, harnessing spatial diversity (§3.1).[3] For practical deployment, commercial chargers can reserve a small portion of FPC space to integrate the sensing coils, without adding extra FPC layers. Each coil connects to its own extractor circuit (Figure 7), including a BAT54s diode package containing the main diode (D) and the auxiliary diode (D_0) for deadzone removal, a capacitor ($C_0 = 1\ \mu$F) for signal amplification, and an RC ($R = 5.6$ kΩ, $C = 10$ nF) for amplitude holder. We implement a 20-kHz sampler to acquire sensing signals from the circuit. The software pipeline, which encompasses data preprocessing and detection, is developed in Python 3.11 using PyTorch and deployed on a Raspberry Pi 4 Model B. We assemble a comprehensive testbed including a diverse set of wireless chargers (Tx), mobile devices (Rx), and metal foreign objects, as illustrated in Figure 12:

- **14 chargers**: Top-selling chargers on Amazon, including a) 13 Qi2-compatible units (10 wireless chargers and 3 charging banks) and b) 1 non-Qi2 charger (Google Pixel Stand).

[3] We fabricated four coils for benchmark evaluation, but MetSentry uses three by default based on the evaluation in §6.3.

Figure 12: Our experimental setup for the evaluation.

- **5 phones**: 4 Qi2-compatible models (iPhone 15 and 16, Samsung Galaxy S26, HMD Skyline) and 1 non-Qi2 phone (Pixel 7 Pro).
- **11 objects**: a) 3 IEC-specified standard foreign objects for safety testing [63] (steel **Disc**, aluminum **Foil**, and aluminum **Ring**) and b) 8 daily objects (Phone **Ring**, **Coin**, **B**utton **Bat**tery, **Key**, paper **Clip**, **S**afety **Pin**, SIM **Eject**or, contactless **Chip** cards).

(2) Data Collection. To train and evaluate MetSentry, we construct training and testing datasets as follows.

Training dataset. Since different wireless charger designs exhibit distinct characteristics, we train one detector per charger type (*i.e.*, brand/model) rather than per physical unit. This enables a manufacturer to train a single detector for a given charger design and deploy it across all units of that product line. For each type, we collect training data and then test the resulting detector with varied phones and objects for cross-domain validation. In total, we collect 2K object-free samples and 2.4K object-present samples across diverse charging conditions, achieving complete model training in only eight hours on an RTX 4060 GPU.

For *object-free samples*, we systematically vary three key factors: device model, device orientation relative to the charger, and phone case presence (with or without). For each device, we record six data traces under diverse conditions (*i.e.*, four orientations and two case states). Recording begins after Tx-Rx power negotiation and transmission power ramp-up by the charger, with each trace lasting 30 seconds at a 20 kHz sampling rate.

For *object-present samples*, we employ only the three IEC-specified foreign objects (steel disc, aluminum foil, and aluminum ring) for training since the detector needs to handle domain shifts during testing (*e.g.*, unseen objects). For each object, we record one 20-second trace in the center region and two 20-second traces at different edge locations (10–20 mm from the center), with randomized device orientations for each session. This results in 9 positive sample traces per Rx, and 36 traces per charger.[4]

Testing dataset. The testing dataset is collected only once to evaluate all chargers. For negative samples, we mirror the training data collection procedure but expand device states to include load variations (standby/light/heavy), battery levels (low/medium/high), device orientation (0–360°), and phone case presence (with/without). For positive samples, we broaden to all 11 objects, consisting of the three IEC-specified foreign objects plus eight unseen daily objects, and position them at diverse locations throughout

[4] Given the limitations of commercial chargers in detecting metal foreign objects, their built-in mechanisms do not interfere, allowing uninterrupted positive sample collection at most cases.

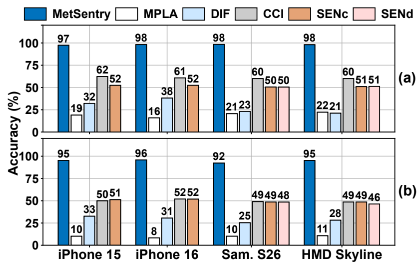

Figure 13: Accuracy of each method across four phones for (a) IEC-specified and (b) non-IEC objects.

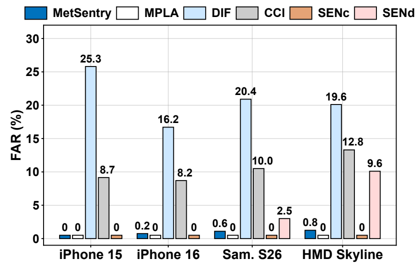

Figure 14: False alarm rate (FAR) of each method across four phones when no foreign object is present.

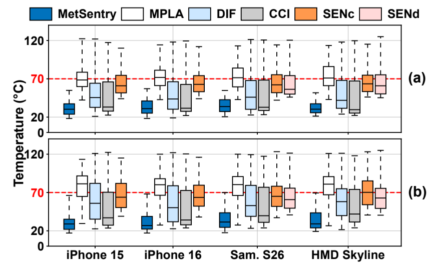

Figure 15: Detection temperature of each method across four phones for (a) IEC-specified and (b) non-IEC objects.

the charging zone with up to five-minute collection per trace, rigorously testing the system performance in the next section.

6 Evaluation

(1) Methods. We compare MetSentry with three methods:

MPLA: The Qi2 standard's prescribed method [32], known as MPP Power Loss Accounting (MPLA), which uses a linear fitting model to estimate charging energy loss and reports a foreign object once the estimated loss exceeds a predefined threshold, promptly halting charging to mitigate risks.

DIF: A state-of-the-art anomaly detection method [57], Deep Isolation Forest (DIF), that integrates isolation forest techniques with deep representation learning. Trained on foreign-object-free charging traces to learn normal electromagnetic patterns, it identifies foreign objects by detecting deviations as anomalies, offering a data-driven alternative to traditional thresholding.

CCI: A parameter estimation-based method [31] that uses the charging-circuit Current Changes as an Indicator (CCI) and employs the current harmonics to guide the threshold setting, triggering detection when the current distortion drops below a threshold.

SENc: A baseline method that uses a surface temperature sensor (a K-type thermocouple) placed on the charger surface for direct temperature monitoring.

SENd: A sensor-based method that uses the smartphone's temperature sensor for detection. Since iOS restricts user access to temperature sensors [1], we only test this method on Samsung Galaxy S26 and HMD Skyline two Android phones. Smartphones have built-in temperature protection mechanisms that limit charging power when the temperature exceeds a threshold (45 °C [13] usually). We also use the same threshold for detection.

(2) Evaluation Metrics. We measure the effectiveness of each method using three main metrics: *Accuracy*: The proportion of cases where foreign objects are correctly detected before the temperature of metal foreign objects reaches 70 °C (the safety thermal threshold specified by IEC). *False alarm rate (FAR)*: The rate of erroneous foreign object declarations when none is present. *Detection temperature*: The foreign object's surface temperature at detection (or peak temperature if undetected), continuously monitored via a K-type thermocouple (K-TC, Figure 12).

6.1 Overall Performance

We first benchmark the three methods on one of the most popular Qi2-compatible wireless chargers, NativeUnion [48], in this subsection. We then extend the evaluation to the other 13 wireless chargers in micro-benchmark evaluations in §6.3.

Accuracy. Figure 13(a) first evaluates detection accuracy on IEC-specified safety-testing objects, which were included in the training. Despite this familiarity, MPLA exhibits limited performance, with accuracy below 25% across all devices. DIF offers marginal gains, as its anomaly detection struggles to extract task-critical features for reliable detection. CCI achieves only modest accuracy (60–62.3%), which is unreliable and suffers from similar issues as the commercial method MPLA. SENc achieves moderate performance, slightly better than SENd, with average detection accuracy of approximately 50%. Because heat decays rapidly with distance and device materials, such temperature-based sensors cannot reliably detect an external metal object. In contrast, MetSentry delivers much stronger results, outperforming MPLA by 75.9–82.3%, DIF by 60.1–77.0%, CCI by 35.1–38.4%, SENc by 51.0–52.4%, and SENd by 45.9–46.9%.

Figure 13(b) further evaluates each method on non-IEC daily objects (entirely **unseen** during training). MPLA remains ineffective, with accuracy dropping close to zero. DIF maintains performance comparable to that in Figure 13(a). CCI, SENc and SENd show degraded performance, yet MetSentry excels, outperforming MPLA by 93.0–95.1%, DIF by 62.0–67.7%, CCI by 42.9–46.5%, SENc by 43.4–47.8%, and SENd by 44.5–48.7%. These results demonstrate that MetSentry is effective in foreign object detection and generalization beyond the training dataset.

False alarm rate (FAR). FAR is measured in foreign-object-free scenarios, eliminating distinctions between IEC and non-IEC objects. As shown in Figure 14, MPLA achieves zero false alarms through its conservative strategy, which prioritizes charging continuity at the expense of detection accuracy. SENc also achieves zero false alarms, as any temperature reading exceeding 65 °C reliably indicates a foreign object—normal smartphones do not reach such temperatures during charging. The other baselines, however, suffer from notable false alarms: DIF (16.2–25.3%) is sensitive to normal charging variations and built-in metallic components; CCI (8.2–12.8%), and SENd (2.5–9.6%) are susceptible to fluctuations in device load and object position. In contrast, in addition to high accuracy, MetSentry reports no false alarms in this experiment, validating the effectiveness of harmonic fingerprints in distinguishing true threats from normal operations.

Detection temperature. Figure 15 reports the surface temperature at which a foreign object is detected. For undetected cases,

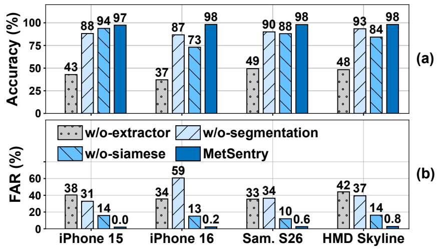

Figure 16: Ablation study using different variants of MetSentry on different mobile phones.

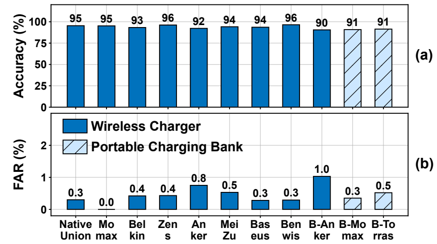

Figure 17: (a) Accuracy and (b) FAR across different wireless chargers and portable charging banks.

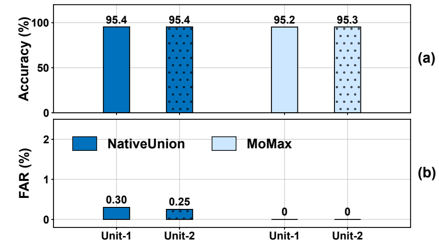

Figure 18: Impact of different units of the same charger on (a) detection accuracy and (b) FAR.

the peak temperature of each trace is recorded to quantify the associated safety risk. For IEC-specified foreign objects, Figure 15(a) reveals that MetSentry detects consistently at much lower temperatures, with an average value of 32.8 °C, safely below the IEC's 70 °C threshold. In contrast, all baselines fall short of this requirement, which have average detection temperatures that are 13.8–40.4 °C higher than MetSentry, with large variance and peaks that sometimes exceed 120 °C. Similar behavior appears for non-IEC objects in Figure 15(b), where MetSentry consistently detects objects at much lower temperatures, offering a clear safety margin.

6.2 Ablation Study

To evaluate the effectiveness of MetSentry's key designs, we perform an ablation study by systematically disabling one key design at a time, leading to three system variants:

- **1) w/o-extractor:** Omits the signal extractor (§3.1), forgoing harmonic fingerprints and instead sampling the raw voltage directly from the sensing coil.
- **2) w/o-segmentation:** Disables signal segmentation in preprocessing (§4.1), replacing it with a fixed-length window of 250 samples.
- **3) w/o-siamese:** Removes the contrastive learning module and replaces the detector (§4.2) by a classic binary classifier using the same backbone as a single Siamese branch without the false-alarm penalty loss to output the detection result directly.

For comparison purposes, we also plot the performance of the full MetSentry in Figure 16. The results show that without the harmonic fingerprint from our signal extractor ("**w/o-extractor**"), accuracy drops sharply to 37.1–49.4%, and FAR rises to 33.4–42.2%, showing the importance of unique fingerprints for reliable detection. Retaining harmonic fingerprinting but lacking segmentation, "**w/o-segmentation**" sustains moderate accuracy (86.7–93.4%) but suffers unreliable outputs with FARs up to 58.7%. Finally, without our contrastive learning-based detection design, "**w/o-siamese**" degrades accuracy by 3.6–25.1% and increases FAR by 9.4–13.9%. Collectively, Figure 16 demonstrates the usefulness and importance of each technical design in MetSentry.

6.3 Micro-benchmarks

We further conduct micro-benchmark experiments to evaluate MetSentry across varied charging scenarios.

Different chargers. To assess MetSentry's adaptability, we evaluate it across a broad spectrum of chargers. Figure 17 presents the accuracy and FAR results for seven additional wireless chargers (Momax, Belkin, Zens, Anker, MeiZu, Baseus, and Benwis) and three wireless charging banks (B-Anker, B-Momax, and B-Torras), as depicted in Figure 12. We can see that MetSentry consistently achieves high accuracy (90.5%–96.5%) while keeping low FAR (0.0%–1.0%). These results demonstrate that MetSentry delivers reliable detection across stationary wireless chargers and portable charging banks, regardless of hardware variations.

We further evaluate the generalization by testing MetSentry on two additional units of two chargers (NativeUnion and Momax), whose data is not used during training. As shown in Figure 18, accuracy and FAR remain consistent across units, indicating that the impact of unit diversity is small to MetSentry.

Number of sensing coils. We investigate the effect of sensing coil count on detection efficacy by varying it from 1 to 4. As shown in Figure 19, expanding coverage and enhancing spatial diversity through sensing coil array dramatically boosts performance, where accuracy increases from 38.2% with one coil to 95.7% with three, while FAR drops from 23.6% to 0.3%. Adding a fourth coil results in marginal declines, likely due to the detector's model capacity constraints in handling expanded features. Thus, MetSentry defaults to three sensing coils in our current development.

Device orientation. To examine the robustness of MetSentry to phone placement orientations, we evaluate it at eight evenly spaced angles (0°/45°/90°/135°/180°/225°/270°/315°). As shown in Figure 20, detection performance remains stable across all orientations, achieving an average accuracy of 95.7% and an average FAR of 0.31%, indicating that device orientation has a minimal impact on the detection performance of MetSentry.

Impact of mobile device states. To examine MetSentry's resilience to dynamic mobile device conditions, we test three key factors that may occur during charging: 1) battery level, 2) device load,[5] and 3) phone case presence. Specifically,

- Battery levels are grouped as low (0–35%), medium (35–70%), and high (70–100%);
- Device loads are categorized as standby, light usage (*e.g.*, chatting or text browsing), and heavy usage (*e.g.*, video recording, gaming, or live streaming); and
- Phone case states encompass with (w/) and without (w/o) cases, including both magnetic and non-magnetic variants.

[5]Different device loads require different power consumption, which in turn can change the working current of the device and affect the coupling of wireless charging.

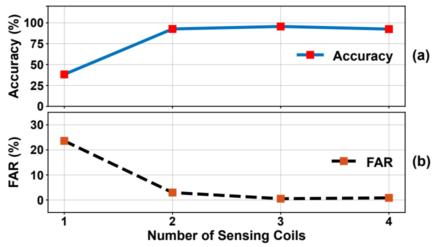

Figure 19: (a) Accuracy and (b) FAR achieved by MetSentry as we increase the number of sensing coils.

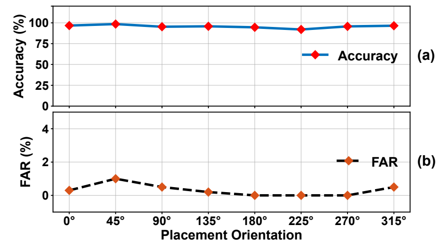

Figure 20: (a) Accuracy and (b) FAR under different device placement orientation angles.

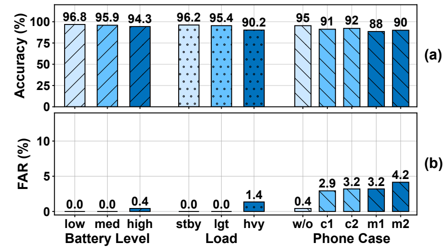

Figure 21: (a) Accuracy and (b) FAR under different device states: battery levels, device loads, and phone cases.

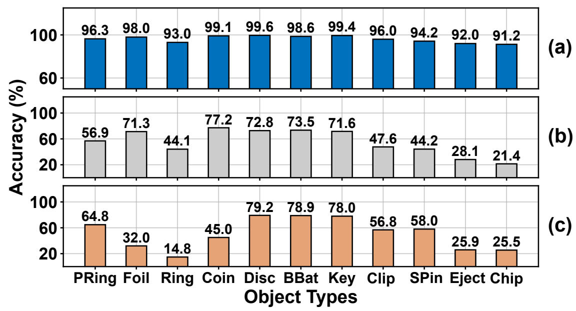

Figure 22: Detection accuracy across various metal foreign object types by (a) MetSentry, (b) CCI, and (c) SENc.

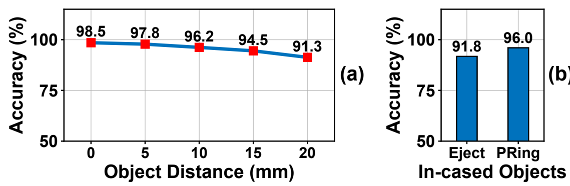

Figure 23: Detection accuracy of MetSentry under varying (a) distances from coil center and (b) in-case concealment

.

Figure 21 shows that across battery levels, accuracy and FAR of MetSentry remain stable, ranging from 94.4–96.8% and 0–0.4%, respectively. A similar trend is observed under different device loads, where performance does not degrade even under heavy usage. Phone cases pose a greater challenge since they affect the charger-device coupling characteristics [19]. We evaluate four cases, including two non-magnetic ones (c1/c2) and two magnetic ones (m1/m2), with the latter introducing additional magnetic pathways. The thicknesses of c1, c2, m1, and m2 are 1 mm, 1.5 mm, 1.8 mm, and 2 mm, respectively. MetSentry maintains good performance, achieving 89–95.4% accuracy with 0.4–4.2% FAR. Magnetic cases with added shielding layers could cause more performance degradation due to increased vertical separation between the charger and the device, attenuating sensing features. In the future, we will improve the performance under such phone cases by jointly optimizing the sensing-coil layout and detection model, and by incorporating calibration or adaptation for more conditions.

Impact of foreign object characteristics. In this experiment, we evaluate MetSentry under varying foreign object types, placements, and in-case concealment. Figure 22 details the detection accuracy for 11 objects, ordered by size from largest (left) to smallest (right). In addition to MetSentry, we also show the performance of CCI (performs best among all baselines without using an extra temperature sensor) and SENc (outperforms another temperature sensor-based method). Object size is an important factor to affect the performance, where smaller objects tend to result in lower detection accuracy, while other factors (besides the detection method itself) may further influence detection, including (1) ferromagnetic materials (*e.g.*, Coin and Disc), which intensify magnetic flux distortion, (2) larger planar conductors (*e.g.*, Key), which enhance eddy current coupling, and (3) hollow structures (*e.g.*, Ring), which reduces coupling area and strength. Overall, the detection accuracies of MetSentry, CCI, and SENc for 11 objects are 91.2–99.6%, 91.2–99.6%, 21.4–77.2%, respectively.

The size of wireless charging area on the charger follows the Qi protocol with a radius of 21.2 mm [51], and we evaluate the impact of object position at 0, 5, 10, 15, and 20 mm from the coil center. Figure 23(a) shows that accuracy decreases gradually from 98.5% (center) to 91.3% (20 mm) as electromagnetic coupling weakens, yet even near the charger edge MetSentry still outperforms all baselines. Figure 23(b) evaluates in-case concealment, where small metal objects (SIM ejector and phone ring) are left inside the phone case during charging. MetSentry detects these concealed objects with 91.8–96% accuracy. These results collectively demonstrate that MetSentry is robust to variations in object type, position, and concealment in real-world scenarios.

Non-Qi2 wireless charging. Proprietary chargers, for specific smartphones, adhere to Qi2 principles but incorporate custom modifications for enhanced charging efficiency, often limiting compatibility to paired devices. Remarkably, MetSentry enhances detection even in these specialized setups. In this experiment, we integrate MetSentry with the Google Pixel Stand for charging its paired phone (Google Pixel 7 Pro), which supports a higher transmission power of 23 W [16]. Figure 24(a) illustrates strong performance across all object types, with accuracy ranging from 91.2–99.6%, and average FAR below 4.2%. This extension beyond standard Qi2 ecosystems demonstrates MetSentry's broad applicability and potential to ensure safety in proprietary charging systems.

6.4 System Overhead

Energy overhead. We employ a Qi2 test module [47] as the receiver, which can stabilize received power at a fixed value (~15 W) for accurate measurements of charging power consumption. We then use a power meter [2] to monitor the charger's input power with and without MetSentry, isolating any incremental draw attributable to MetSentry. As illustrated in Figure 24(b), the added

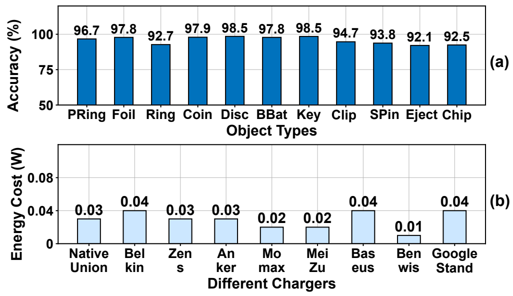

Figure 24: (a) Performance on a non-Qi2 charger; (b) Energy overhead across each charger.

power consumption ranges from just 0.01–0.04 W, corresponding to a negligible 0.6–2.6‰ increase across various wireless chargers.

Memory and latency overhead. We evaluate MetSentry's memory and latency on a Raspberry Pi 4, where our lightweight software pipeline consumes only 8.3 MB of memory. Within a 300-ms buffer (default configuration in MetSentry), there are typically 1–3 packets. Segmentation takes 64.9 ms, and inference (batch processing across three sensing coils) takes 49.7 ms per packet, resulting in a total processing time of 114.6–214.9 ms. The processing is lightweight and can be completed before the signal fills the next buffer.

6.5 Deployment Cost Discussion

Finally, we discuss the hardware and software costs of the current MetSentry design when it is integrated into wireless chargers.

Hardware cost. The additional hardware includes a sensing coil array (copper traces on a flexible PCB) and an extraction circuit (diode, capacitors, and resistors), totaling approximately $5 per unit in our prototype. For production, the sensing coils can be integrated into the charger's existing PCB layout or fabricated on a thin FPC layer, with cost reductions expected at scale. Note that no modification to mobile devices is required.

Software cost. The detector software runs on the processor of the wireless charger. For embedded deployment, the detector model (~52,890 parameters) requires only ~1.84 M multiply-accumulate operations per detection, with a peak memory of about 230 KB in float32, which is feasible on MCUs such as the STM32H7 series (480 MHz, 1 MB RAM). With int8/int16 quantization, memory reduces to 64–115 KB, fitting even lower-cost MCUs with 512 KB SRAM at less than 1 W power consumption. We will integrate pruning and quantization into MetSentry in future work of this paper.

7 Related Work

Foreign object detection for mobiles. Existing detection methods primarily track electrical parameters of wireless charging systems that metal foreign objects can influence, such as circuit voltage [38], resonance frequency [21], current [26], and signal quality indicator [14]. However, these threshold-based approaches are highly susceptible to misalignment between the charger and mobile device [15, 33]. A recent work [31] uses the current changes in the charging circuit as an indicator and adopts the current harmonics to guide the threshold setting, which still belongs to the existing threshold-based methods and has their inherent limitations (§6). To address this, the latest Qi2 protocol employs magnets for precise alignment [10, 20]. Earlier commercial solutions inject pulse signals and monitor their oscillation decays [27], but these are limited to open-circuit conditions and fail to provide continuous monitoring during charging [14]. Therefore, the dominant approach today monitors energy loss [32]. Yet, energy loss can be affected by many factors related to devices, metal objects, and environments, which is challenging to quantify in practice [64]. In contrast, MetSentry explores a unique fingerprint of metal foreign objects without knowing device- or object-specific parameters.

Wireless charging in other scenarios. Beyond mobiles, wireless charging is increasingly adopted for high-power applications in autonomous systems like robots, drones, and electric vehicles, which often involve larger air gaps [7, 43]. In these charging systems, metal foreign object detection is equally vital for safety. Unlike the inductive coupling used in mobile phones, which demands close proximity for efficiency [22], these systems employ resonant coupling to accommodate greater separation between charger and device [42]. As a result, detection methods in these domains often rely on specialized sensors, such as thermal imaging [45] or hyperspectral cameras [46] to detect temperature anomalies from eddy currents and wave-based techniques [3, 11] using modulated electromagnetic waves for metallic object detection. Other approaches deploy auxiliary sensors to monitor coupling strength variations caused by foreign objects [44, 53]. However, these methods demand bulky hardware and large air gaps between transmitter and receiver, making them unsuitable for mobile wireless charging.

Assorted sensing and learning technologies. Recent research has harnessed electromagnetic field signals for human-related sensing [5, 18] and uncovering security flaws in wireless systems [28, 58, 61]. Electromagnetic signals have also been utilized for localization [29, 54] and communication [37]. The harmonic fingerprints that MetSentry exploits for foreign object detection remain unexplored, yet our analysis and processing of wireless charging signals may help further improve these designs. In addition, prior works have successfully applied classification models [4, 49, 55] and learning techniques [36, 56, 59] for sensing tasks. MetSentry builds upon these advancements by designing a streamlined architecture that achieves reliable generalization without extensive training data.

8 Conclusion

This paper presents MetSentry, a novel co-designed solution of hardware and software that achieves reliable metal foreign object detection in mobile wireless charging. By exploiting the key observation that metal foreign objects disproportionately attenuate high-frequency harmonics, *i.e.*, effectively acting as a low-pass filter on electromagnetic field signals, MetSentry captures this fingerprint for reliable metal foreign object detection in wireless charging. Extensive evaluations across diverse chargers, smartphones, and foreign objects demonstrate that MetSentry significantly outperforms existing built-in and state-of-the-art methods.

Acknowledgments

Zhenjiang Li is supported by the GRF grant from the Research Grants Council of Hong Kong (CityU 11205624). Hao Zhou and Xinyu Wang are supported by China National Natural Science Foundation under Grant 625B2174. Corresponding authors: Hao Zhou and Zhenjiang Li.

References

[1] Apple Developer Documentation. 2025. https://developer.apple.com/documentation/foundation/processinfo/thermalstate-swift.enum.

[2] Bi-directional Current Detection. 2025. https://www.chargerlab.com/.

[3] Alberto Garcia Briz, Andrew M Gilbert, and Grzegorz Ombach. 2017. Methods and systems for object detection and sensing for wireless charging systems. US Patent 9,735,605.

[4] Jiani Cao, Jiesong Chen, Chengdong Lin, Yang Liu, Kun Wang, and Zhenjiang Li. 2024. Practical Gaze Tracking on Any Surface With Your Phone. *IEEE Transactions on Mobile Computing* (2024).

[5] Jiani Cao, Yang Liu, Lixiang Han, and Zhenjiang Li. 2024. Finger tracking using wrist-worn EMG sensors. *IEEE Transactions on Mobile Computing* (2024).

[6] Lili Chen, Bozhong Yu, Yongjian Fu, Ju Ren, Hao Pan, Jeremy Gummeson, and Yaoxue Zhang. 2024. Pushing wireless charging from station to travel. In *Proc. of ACM MobiCom*.

[7] Lili Chen, Yizhe Zhao, Shuning Wang, Linghui Zhong, Yongjian Fu, Sheng Yue, Ju Ren, and Yaoxue Zhang. 2025. Towards Distance-Adaptive Wireless Charging. In *Proc. of ACM MobiSys*.

[8] International Electrotechnical Commission. 2018. Audio/video, information and communication technology equipment - Part 1: Safety requirements. IEC 62368-1:2018. Section 9.6.2 Specification of the foreign objects.

[9] Wireless Power Consortium. 2022. System Description Wireless Power Transfer, v1.3. https://www.wirelesspowerconsortium.com/qi-authentication/.

[10] Wireless Power Consortium. 2024. Qi Specification Version 2.0. https://www.wirelesspowerconsortium.com/media/52oflpuk/qi-v20-public.zip.

[11] Teodor Cretu, Zachary Molseed, Jonathan Gooch, Girma Tewolde, and Chen Duan. 2025. Wireless Qi-charged AGV Navigation and Voltage Sensor Fusion for Coil Alignment-targeted Auto-parking and Foreign Object Detection. In *Proc. of IEEE WPTCE*.

[12] Minhao Cui, Binbin Xie, Qing Wang, and Jie Xiong. 2023. Dancingant: Body-empowered wireless sensing utilizing pervasive radiations from powerline. In *Proc. of ACM MobiCom*.

[13] Does excess heat damage your phone? 2024. https://www.telstra.com.au/exchange/can-heat-damage-your-phone.

[14] Shinichi Fukuda, Hiroaki Nakano, Yuji Murayama, Tomomichi Murakami, Osamu Kozakai, and Kenichi Fujimaki. 2012. A novel metal detector using the quality factor of the secondary coil for wireless power transfer systems. In *Proc. of IEEE IMWS*.

[15] Yunyi Gong, Yoshitsugu Otomo, and Hajime Igarashi. 2022. Neural Network for Both Metal Object Detection and Coil Misalignment Prediction in Wireless Power Transfer. *IEEE Transactions on Magnetics* (2022).

[16] Google Pixel Stand (2nd gen). 2025. https://store.google.com.

[17] David J Griffiths. 2023. *Introduction to electrodynamics*. Cambridge University Press.

[18] Xiuzhen Guo, Long Tan, Tao Chen, Chaojie Gu, Yuanchao Shu, Shibo He, Yuan He, Jiming Chen, and Longfei Shangguan. 2024. Exploring biomagnetism for inclusive vital sign monitoring: Modeling and implementation. In *Proc. of ACM MobiCom*.

[19] Iftikhar Hussain and Dong-Kyun Woo. 2022. Simplified mutual inductance calculation of planar spiral coil for wireless power applications. *Sensors* (2022).

[20] Ushering in the New Wireless Charging Era with Qi v2.1. 2025. https://www.graniteriverlabs.com/en-us/technical-blog/beyond-qi2-wireless-charging.

[21] Hassan Jafari, Masood Moghaddami, and Arif I Sarwat. 2019. Foreign object detection in inductive charging systems based on primary side measurements. *IEEE Transactions on Industry Applications* (2019).

[22] Shenyao Jiang, Hao Zhou, Wangqiu Zhou, Xinyu Wang, Zhenjiang Li, and Yusheng Ji. 2025. FreAuth$^+$: A Robust Frequency Feature-Based Device Authentication Mechanism for Magnetic Wireless Power Transfer System. *IEEE Transactions on Mobile Computing* (2025).

[23] Neil Kuyvenhoven, C Dean, J Melton, J Schwannecke, and AE Umenei. 2011. Development of a foreign object detection and analysis method for wireless power systems. In *Proc. IEEE ISPCE*.

[24] Eun S Lee. 2024. Editorial on Wireless Power Transfer (WPT): Present advancements, applications, and future outlooks.

[25] Jiachun Li, Yan Meng, Le Zhang, Guoxing Chen, Yuan Tian, Haojin Zhu, and Xuemin Sherman Shen. 2023. MagFingerprint: A Magnetic Based Device Fingerprinting in Wireless Charging. In *Proc. of IEEE INFOCOM*.

[26] Sheng Li, Haoze Li, Zhijun Wu, Guangjie Bao, Kejun Qian, and Yafei Li. 2021. Foreign Object Detection for LCC-S Wireless Power Transfer System Based on LSTM. In *Proc. of IEEE ICESIT*.

[27] Xun Liu, Laurens Henricus Swaans, Ka Wai Paul Chan, Ho Kan Low, and Wing Kwong Chan. 2015. Methods and systems for detecting foreign objects in a wireless charging system. US Patent 9,178,361.

[28] Yihao Liu, Kai Huang, Xingzhe Song, Boyuan Yang, and Wei Gao. 2020. Maghacker: eavesdropping on stylus pen writing via magnetic sensing from commodity mobile devices. In *Proc. of ACM MobiSys*.

[29] Chris Xiaoxuan Lu, Yang Li, Peijun Zhao, Changhao Chen, Linhai Xie, Hongkai Wen, Rui Tan, and Niki Trigoni. 2018. Simultaneous localization and mapping with power network electromagnetic field. In *Proc. of ACM MobiCom*.

[30] Jianghua Lu, Guorong Zhu, and Chunting Chris Mi. 2022. Foreign Object Detection in Wireless Power Transfer Systems. *IEEE Transactions on Industry Applications* (2022).

[31] Phemelo Maile and Sampath Jayalth. 2025. Foreign Object Detection Using Total Harmonic Distortion of Input Current. In *2025 IEEE Wireless Power Technology Conference and Expo (WPTCE)*.

[32] LQK Measurements & More New Qi2 Compliance Features 2024: Foreign Object Detection. 2024. https://www.graniteriverlabs.com/en-us/technical-blog/2024-qi2-technical-compliance.

[33] Songyan Niu, Cheng Zhang, Yujun Shi, Shuangxia Niu, and Linni Jian. 2022. Foreign object detection considering misalignment effect for wireless EV charging system. *ISA transactions* (2022).

[34] Standardization Administration of the People's Republic of China. 2020. Electric Vehicle Wireless Power Transfer - Part 1: General Requirements, State Administration for Market Regulation. GB/T 38775.1.

[35] Masaya Ote, Soyeon Jeong, and Manos M Tentzeris. 2020. Foreign object detection for wireless power transfer based on machine learning. In *Proc. of IEEE WPTC*.

[36] Xiaomin Ouyang, Xian Shuai, Jiayu Zhou, Ivy Wang Shi, Zhiyuan Xie, Guoliang Xing, and Jianwei Huang. 2022. Cosmo: contrastive fusion learning with small data for multimodal human activity recognition. In *Proc. of ACM MobiCom*.

[37] Dilushi Piumwardane, Madhushanka Padmal, Kasun Hewage, Vaishnavi Ranganathan, and Thiemo Voigt. 2023. Towards Low-cost Sensing with Mobile Backscatter. In *Proc. of ACM MobiCom*.

[38] Nunzio Pucci, Juan M Arteaga, Christopher H Kwan, David C Yates, and Paul D Mitcheson. 2021. Induced voltage estimation from class ef switching harmonics in hf-ipt systems. *IEEE Transactions on Power Electronics* (2021).

[39] Qi Wireless Charging Market Growth Forecast. 2025. https://www.newstrail.com/qi-wireless-charging-market-growth-forecast-size-share-and-industry-trends-2025-2032/.

[40] RC time constant and diode detector. 2025. https://electronics.stackexchange.com/questions/100518/rc-time-constant-and-diode-detector.

[41] Paul Scherz. 2006. *Practical electronics for inventors*. McGraw-Hill, Inc.

[42] Lixin Shi, Zachary Kabelac, Dina Katabi, and David Perreault. 2015. Wireless power hotspot that charges all of your devices. In *Proc. of ACM MobiCom*.

[43] Zhuouqun Shi, Qianfang Sun, Jintao Wang, and Zhizhen Liu. 2024. Free-Position Dynamic WPT System Supporting InFlight Concurrent Charging for Multiple Unmanned Aerial Vehicles. *IEEE Transactions on Power Electronics* (2024).

[44] Huishu Song, Xiaosheng Huang, Shuyi Lin, Ruping Lin, and Jing Huang. 2023. A Flexible Foreign Object Detection Method Based on Arrayed Vertical-Decoupled Coils for Wireless Power Transfer Systems. In *Proc. of IEEE ICWPT2022*.

[45] Ying Sun, Guo Wei, Kai Song, Xiaohua Huang, Qian Zhang, and ChunBo Zhu. 2020. Determination foreign object detection area in electric vehicle wireless charging system based on thermal temperature rise characteristic. In *Proc. of IEEE ITEC*.

[46] Yong Tian, Zheng Li, Yawen Lin, Lijuan Xiang, Xiaoyu Li, Yonghong Shao, and Jindong Tian. 2021. Metal object detection for electric vehicle inductive power transfer systems based on hyperspectral imaging. *Measurement* (2021).

[47] Unboxing of ChargerLAB POWER-Z Q25 Qi2 Tester. 2025. https://www.chargerlab.com/unboxing-of-chargerlab-power-z-q25-qi2-tester/.

[48] Voyage 2-in-1 Magnetic Wireless Charger. 2025. https://www.nativeunion.com/products/.

[49] Yanwen Wang, Jiaxing Shen, and Yuanqing Zheng. 2020. Push the limit of acoustic gesture recognition. *IEEE Transactions on Mobile Computing* (2020).

[50] Wireless Charging Market. 2025. https://www.precedenceresearch.com/wireless-charging-market.

[51] Wireless Power Consortium. 2021. *Qi Specification Version 2.2.1 – MPP System.* Technical Specification. Wireless Power Consortium. https://www.wirelesspowerconsortium.com/knowledge-base/qi-specification/download-the-qi-specifications/ Section 4, Coil Design, p. 31.

[52] Yi Wu, Zhuohang Li, Nicholas Van Nostrand, and Jian Liu. 2021. Time to rethink the design of qi standard? security and privacy vulnerability analysis of qi wireless charging. In *Proc. of ACM ACSAC*.

[53] Chenyang Xia, Chenhao Lu, Shuze Zhao, Ziyue Yang, Yuheng Cao, Fuqian Liu, and Yuxiang Gao. 2024. Planar double-winding foreign object detection for the EV wireless charging system based on time-division multiplexing. *IEEE Transactions on Power Electronics* (2024).

[54] De Xiao Xia, Jia Qi Han, Ya Jie Mu, Lei Guan, Xin Wang, Xiang Jin Ma, Li Hao Zhu, Tian Guang Lv, Hai Xia Liu, Yan Shi, et al. 2024. Adaptive wireless-powered network based on CNN near-field positioning by a dual-band metasurface. *Nature Communications* (2024).

[55] Zhiyuan Xie, Xiaomin Ouyang, Li Pan, Wenrui Lu, Guoliang Xing, and Xiaoming Liu. 2023. Mozart: A mobile tof system for sensing in the dark through phase manipulation. In *Proc. of MobiSys*.

[56] Huatao Xu, Liying Han, Qirui Yang, Mo Li, and Mani Srivastava. 2024. Penetrative ai: Making llms comprehend the physical world. In *Proc. of ACM HotMobile*.
[57] Hongzuo Xu, Guansong Pang, Yijie Wang, and Yongjun Wang. 2023. Deep Isolation Forest for Anomaly Detection. *IEEE Transactions on Knowledge and Data Engineering* (2023).
[58] Mingming Xu, Yinghui He, Xin Li, Jingzhi Hu, Zhe Chen, Fu Xiao, and Jun Luo. 2024. Beamforming made Malicious: Manipulating Wi-Fi Traffic via Beamforming Feedback Forgery. In *Proc. of ACM MobiCom*.
[59] Xiangyu Xu, Jiadi Yu, Yingying Chen, Qin Hua, Yanmin Zhu, Yi-Chao Chen, and Minglu Li. 2020. TouchPass: Towards behavior-irrelevant on-touch user authentication on smartphones leveraging vibrations. In *Proc. of ACM MobiCom*.
[60] Lanqing Yang, Yi-Chao Chen, Hao Pan, Dian Ding, Guangtao Xue, Linghe Kong, Jiadi Yu, and Minglu Li. 2020. MagPrint: Deep Learning Based User Fingerprinting Using Electromagnetic Signals. In *Proc. of IEEE INFOCOM*.
[61] Sihan Yu, Jingjing Fu, Chenxu Jiang, Chunchih Lin, Zhenkai Zhang, Long Cheng, Ming Li, Xiaonan Zhang, and Linke Guo. 2024. FreeEM: Uncovering parallel memory EMR covert communication in volatile environments. In *Proc. of ACM MobiSys*.
[62] Zihao Zhan, Yirui Yang, Haoqi Shan, Hanqiu Wang, Yier Jin, and Shuo Wang. 2024. VoltSchemer: Use Voltage Noise to Manipulate Your Wireless Charger. In *Proc. of USENIX Security*.
[63] Shun Zhang, Yingchun Shu, Daniel Barsotti, and Gary Gray. 2019. Thermal Considerations for Information Technology Equipment from Product Safety Perspective. In *Proc. of IEEE SPCE Austin*.
[64] Yiming Zhang, Zhengchao Yan, Jiaqi Zhu, Siqi Li, and Chris Mi. 2019. A review of foreign object detection (FOD) for inductive power transfer systems. *ETransportation* (2019).

Temporary page!

LaTeX was unable to guess the total number of pages correctly. As there was some unprocessed data that should have been added to the final page this extra page has been added to receive it.

If you rerun the document (without altering it) this surplus page will go away, because LaTeX now knows how many pages to expect for this document.